crystals

MDPI

Article

Crystallographic and Geometric Factors in the Shear Development in <001> FCC Single Crystals: Molecular Dynamics Simulation and Experimental Study

Dmitry V. Lychagin [1], Andrey I. Dmitriev [1,2,*], Anton Yu. Nikonov [1,2] and Ekaterina A. Alfyorova [3]

[1] TSU Tomsk State University, Lenin av. 36, 634050 Tomsk, Russia; dvl-tomsk@mail.ru (D.V.L.); anickonoff@ispms.ru (A.Y.N.)

[2] ISPMS Institute of Strength Physics and Material Science SB RAS, Akademicheskii pr. 2/4, 634055 Tomsk, Russia

[3] TPU National Research Tomsk Polytechnic University, Lenin av. 30, 634050 Tomsk, Russia; katerina525@mail.ru

* Correspondence: dmitr@ispms.ru; Tel.: +7-3822-286-826

Received: 23 June 2020; Accepted: 25 July 2020; Published: 2 August 2020

Abstract: An approach to the study of the mechanisms of shear deformation in the bulk of face centered cubic (FCC) single crystals based on molecular dynamics simulation is proposed. Similar shear patterns obtained experimentally, and in simulations, allow consideration of the effect of crystallographic and geometric factors on deformation mechanisms. Deformation of <001> single-crystal samples in the form of tetragonal prisms with {110} and {100} lateral faces and different height-to-width ratios was studied. The simulation showed that the sample vertices are the preferential sites for shear initiation. It was found that the formation of deformation domains and interaction of shear planes are caused by the geometry of shear planes in the bulk of the single crystal, i.e., by their location in relation to basic stress concentrators and by their orientations relative to the lateral faces. The deformation patterns obtained in the simulations were in good agreement with those observed in the experiments. The fractions of sliding dislocations and dislocation barriers were determined for different materials, taking into account the crystallographic and geometric factors.

Keywords: single crystal; shear; geometric factors; molecular dynamics simulation; deformation development

1. Introduction

When studying the mechanical behavior of materials subjected to plastic deformation, the main focus is on the determination of the yield strength and the analysis of strain hardening and plasticity. Dislocation glide within grains of polycrystals is usually distinguished from dislocation transmission through grain boundaries. It is reasonable to study the intragranular deformation mechanisms using single crystals that make it possible to calculate the shear stress given the direction of an applied load. In many cases a single crystal is considered to be homogeneous, with deformation propagating through the activation of heavily loaded sliding systems. It is supposed that the uniformly loaded systems can be activated throughout the entire bulk of the crystal. Meanwhile, deformation of a single crystal subjected to uniaxial compression (free settling) is noticeably inhomogeneous even for high symmetry orientations. The deformation non-uniformity is affected by the distribution irregularity of external stresses caused by the geometric shape of a

sample and by the difference in shear conditions along various directions, in particular, towards the sample lateral surfaces or the punches of the testing machine. In addition, the axial symmetry of the stress field requires uniform deformation of the sample towards its lateral surfaces. This results in transformation from initial "uniform" deformation of the sample to consistent deformation of macro- and mesovolumes. It is evident from crystallographic and geometric considerations that changes in the shape and height of single crystals should also affect the deformation. The changes in sample geometry and crystallographic orientations of the axis of compression and the lateral surfaces induce the alteration of the number of the slip systems oriented towards the sample lateral surfaces or the punches of the testing machine. Moreover, it is necessary to consider the difference in the principal stress patterns in the near-face regions and in the middle of the sample caused by the friction force as well as their variations at different height-to-width ratios. These characteristic features of deformation have been studied in single crystals of face centered cubic (FCC) metals and single-phase alloys [1]. The elements of the deformation relief in these materials have been classified in [2].

The most effective and informative method to study local deformation of single crystals is a digital image correlation (DIC) method [3–6]. Electron back scattering diffraction (EBSD) [7–9] and X-ray diffraction analysis with a focused spot [5] are extensively used to investigate deformation related reorientation. It has been clearly shown that the shape changes of a material subjected to loading whilst maintaining its integrity are provided by its decomposition into deformation domains followed by their consistent deformation [3,5,9–11].

Despite the recent progress, the experimental techniques of deformation relief examination are unable to unambiguously interpret shear patterns in the bulk of a single crystal. The analysis of these processes is possible only by means of computer simulation. The simulation makes it possible not only to implement atomic shear along octahedral planes but also to distinguish the contributions of each factor affecting the evolution of the deformation relief. In particular, such an approach can be realized by molecular dynamics (MD). Currently this method is successively used to solve a wide range of atomic scale issues in single crystals. Most often such works focus on studying the evolution of plastic deformation under tension–compression [12–18], torsion [19], different surface loads: nanoindentation [20], burnishing [21], scratching [22–25], cutting [26–28], etc. In particular, the effect of elastic anisotropy in a Cu single crystal subjected to compression/tension and the dependence of its yield strength on the crystallographic orientation and the loading direction were studied by MD simulation [12]. In [18] this method was used to investigate the mechanism of the homogenous dislocation nucleation stress asymmetry under applied uniaxial tensile and compressive loads in various FCC single crystals. Rawat et al. studied the evolution of compression twinning and dislocations under uniaxial stress conditions in a hexagonal close-packed (HCP) rystal structure [17]. The motion of an individual screw dislocation in a copper single crystal was studied in [29]. The effect of crystallographic orientation of Cu single crystals on their nanocutting was revealed in [28], while the process of material removal in single-crystal copper with rough surfaces subjected to nanoscale scratching was studied in [22,23]. Molecular dynamics simulations were also employed to study the nanometric machining process of single crystal nickel [30] and the effect of the crystallographic orientation of Ti grains on their strain hardening under scratching. This method provides observation of local structural changes in different deformed solids. In particular, the nucleation mechanisms of shear bands in amorphous materials [31,32] and deformation behavior of twinned body-centered cubic (BCC) nanowires under uniaxial compression [33] were investigated with MD simulation. Despite the wide range of issues concerned with crystallographic anisotropy, which are treated by MD, the issues related to evolution of deformation relief in single crystals remained to be resolved. Therefore, the present work is focused on an MD study of shear deformation in microvolumes of <001> FCC single crystals with different height-to-width ratios and crystallographic orientations of the lateral faces (geometric and crystallographic factors), and on the comparison of the simulation results with experimentally observed deformation relief taking into account self-similarity of the processes.

2. Materials and Geometric Analysis of Shear Crystallography

Single-crystal samples in the form of a tetragonal prism representing a metal with a face centered cubic (FCC) lattice were subjected to uniaxial tension in the MD simulations to analyze the evolution of the deformation relief. The strain axis of the single crystals was aligned along the <001> direction. The lateral faces of the samples were {110} and {100} planes. The height-to-width ratio h/d in the samples was set as h/d = 2 and h/d = 1. The orientations of the octahedral shear planes relative to the lateral faces and close-packed directions of the single crystals, as well as to the punches of the testing machine, are shown in Figure 1.

It can be seen from Figure 1a that for the sample with h/d = 2 and {110} lateral faces one can distinguish a region (designated as V_0), where slip planes appear on both lateral faces. In the rest volume of the sample designated as V_1 the shear planes appeared on the one of the lateral faces in the area covered by the punch of the testing machine. It should be noted that the volume V_0 increased for the samples with h/d > 2. For the crystal with cubic lateral faces and h/d = 2, the volume V_0 diminished to a one plane. At h/d > 2 the plane was changed to the volume V_0. The shadowed plane in Figure 1b separates the volumes V_1 each of which borders with one of the punches of the testing machine.

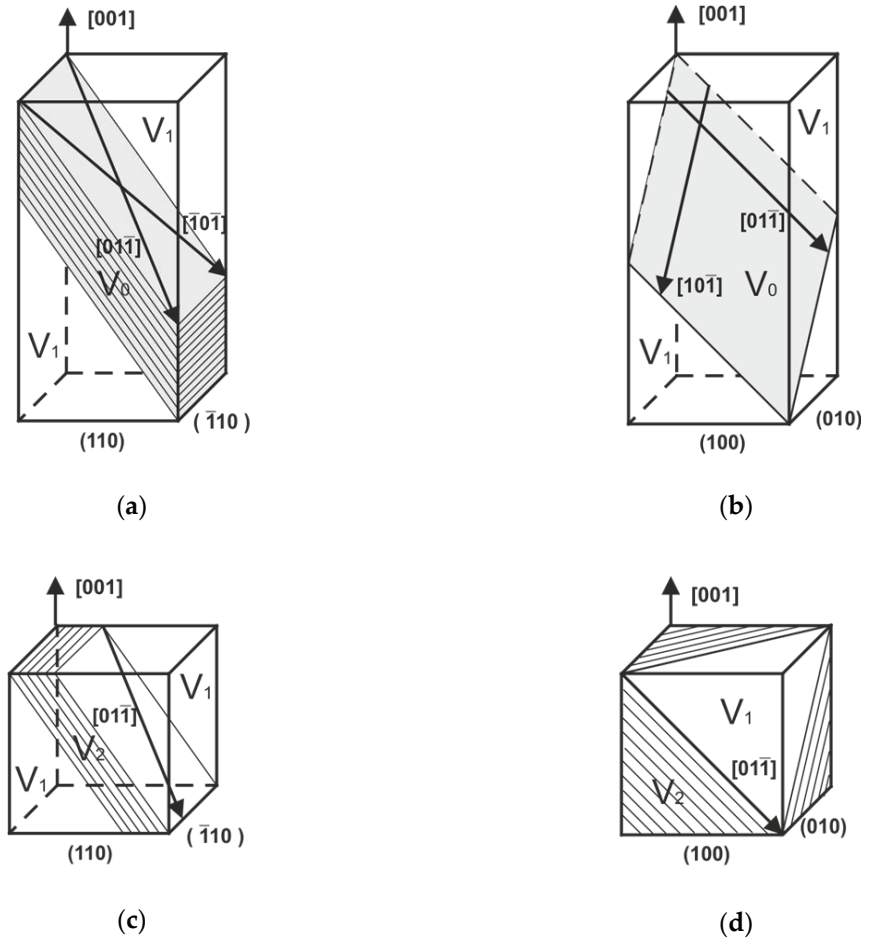

Figure 1. Schematic showing orientations of octahedral plane families in [001] single crystals with (**a**,**b**) h/d =2; (**c**,**d**) h/d =1 and (**a**,**c**) {110} or (**b**,**d**) {100} lateral faces.

Shear conditions in the considered volumes were different. In the volume V_1 the shear occurred easily only from the punch towards the lateral face. In contrast, in the volume V_0 the shear was possible in the forward and backward directions. As can be seen, some of the shear planes came out on two lateral faces of the sample, whereas the others appeared on only the one face, while from the other side the shear plane was bordered by the top surface. Evidently, the contribution of these shear

directions to the deformation of the sample would be different. The volume V_0 was characterized by maximum deformability. Deformation in this volume was visualized as a shear band propagating through a family of parallel planes.

When decreasing the sample height, the volume V_0 disappeared at the critical values $h_{cr} = 1.43d$ in the single crystals with {110} lateral faces and $h_{cr} = 2d$ in those with {100} lateral faces. A sample height lower than h_{cr} resulted in the appearance of the volume V_2 that bordered with the punches of the testing machine on both sides (Figure 1c,d). Shear in this volume was impeded due to the backward stresses induced by the opposite punch. It was possible only in some parts of the volume defined by close-packed directions in the shear plane and was directed towards the lateral faces of the crystal.

Thus, the three distinctive volumes V_0, V_1 and V_2, differing by orientations of the octahedral slip planes relative to the punches of the testing machine and the lateral faces of the sample, can be marked out in the studied single crystals. Due to various possible shear patterns in these volumes, the observation of different strain-relief patterns in the volumes and in the single crystal as a whole was expected. The present analysis was performed for the only one chosen octahedral shear plane. However, the single crystals with such orientation were characterized by four octahedral shear planes with two shear directions in each plane, i.e., by eight equiloaded shear systems with a Schmid factor of 0.41. The planes were located symmetrically with regard to a vertical 4-fold axis (axis of loading). Therefore, the volumes had smaller dimensions. Their locations were determined by all the four equiloaded planes. The geometric shape of these volumes determined different slip patterns in local regions. This, in turn, governed the location of deformation domains in the bulk of the single crystal.

Along with crystal geometric consideration of deformation, as mentioned above, when analyzing strain conditions, it is necessary to take into account the pattern of principal stresses in local regions of the single crystal and their variation on decreasing the sample height. Our calculations showed [34] that in the case of end-face friction the eight sample vertices were the sites of high stress concentration (basic concentrators). Therefore, slip should be primarily initiated from the vertices that should be considered in the analysis of the simulation results.

3. The Model Sample Description

MD calculations of evolution of atomic configurations in the single crystals subjected to uniaxial tension were implemented using the LAMMPS [35] (Large-scale Atomic/Molecular Massively Parallel Simulator) molecular dynamics code. LAMMPS integrates Newton's equations of motion for an ensemble of atoms or molecules that interact via short- or long-range forces with a variety of initial and boundary conditions. The model sample consisted of FCC metal atoms (aluminum and nickel) with an interatomic potential reconstructed in the framework of the embedded atom method (EAM) [36]. The equations of motion were integrated on the basis of the Velocity-Verlet algorithm. To analyze and visualize the defects of crystal structure the open visualization tool OVITO [37] was used. The simulated sample was considered as an NVE ensemble, which maintains the number of atoms N, the occupied volume V and the energy of the system E. Physical correctness of the software program was verified by matching the calculated and experimental values of vacancy and stacking fault formation energies. The mismatch achieved was less than 1%.

Two kinds of the samples with different h/d ratios were simulated. The crystallite with h/d = 2 had the shape of a parallelepiped with dimensions of 30×60×30 lattice parameters along the X, Y and Z directions, respectively. The sample with h/d = 1 was represented by a cube with the dimensions along the X, Y and Z directions set as 30×30×30 lattice parameters. Uniaxial compression of the crystallites along the Y axis was simulated by moving two additional planes located above and below the sample along the Y axis. As shown in Figure 2a, the upper plane moved with a constant speed of -2.5 m/s, while the speed of the lower one was 2.5 m/s. The thickness of the planes was 3 lattice parameters, while their dimensions along the X and Z axes were 60 lattice parameters. During loading the distance between atoms in the planes was fixed constant that simulates compression of the sample by two rigid punches. Free boundary conditions were set along X and Z directions. The

strain was calculated as $dh/h_0 \cdot 100\%$, where h_0 is the initial sample height, and dh is the total distance travelled by the planes. The Common Neighbor Analysis (CNA) and Dislocation Extraction Algorithm (DXA) implemented in the OVITO software [38] were used to identify crystal lattice defects during uniaxial compression. In particular, the types of planar defects were determined based on the analysis of atomic arrangement of neighboring planes (Figure 2b), namely an HCP–HCP arrangement was attributed to an intrinsic stacking fault (ISF), an HCP–FCC–HCP arrangement was assigned to an extrinsic stacking fault (ESF), and an FCC–HCP–FCC arrangement was ascribed to a twin boundary (TB). The initial temperature of the samples was set to 5 K. The low temperature was chosen in order to ease the observation of lattice defects. On the other hand, the choice of a non-zero initial temperature was explained by the necessity of the presence of indeterminate oscillations of atoms caused by thermal fluctuations.

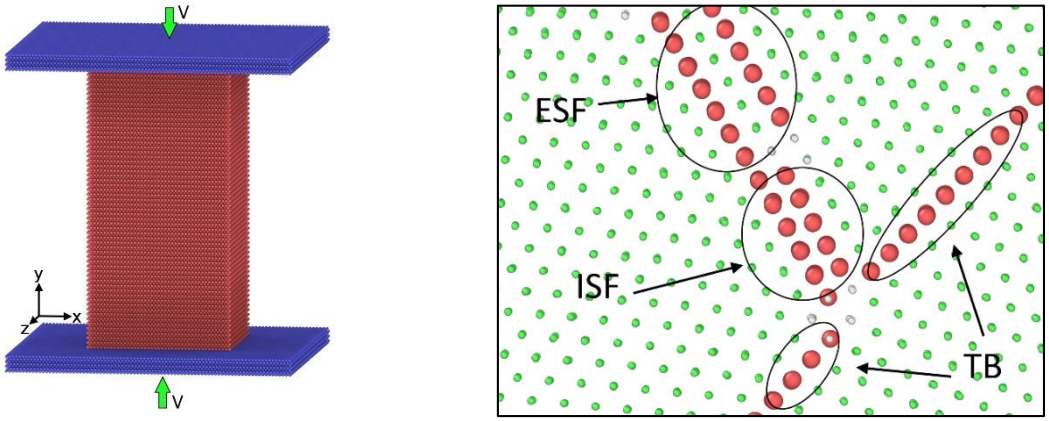

(**a**) (**b**)

Figure 2. (**a**) Schematic showing the modeled crystallite with h/d = 2; (**b**) crystallite fragment containing intrinsic stacking fault, extrinsic stacking fault and twin boundary. Common Neighbor Analysis (CNA) was used to visualize the defects: hexagonal close-packed (HCP) atoms are shown as red dots and face centered cubic (FCC) atoms are indicated as green dots.

4. Simulation Results and Comparison with Experiment

4.1. Single Crystals with the <001> Axis of Compression and {110} Lateral Faces

4.1.1. Sample with h/d = 2

The simulation showed that shear initiated at all the eight vertices of the nickel sample through simultaneous generation of Shockley partial dislocations with the Burgers vector 1/6<112> (colored green in Figure 3 and thereafter). These dislocations resulted in the formation of intrinsic stacking faults. It should be noted that the dislocations glided from each vertex along two conjugate shear planes (Figure 3a,b). Therefore, dislocation movement from one slip plane to another and interaction of dislocations gliding along different slip planes were highly probable. These effects can result in the formation of a stair-rod dislocation along the intersection line of the planes. The simulation revealed that it was the 1/3<001> Hirth type dislocation. The following deformation looked like a shear of the plane, which was activated along both directions. However, actually, the deformation occurred by activation of two different shear systems acting in two close parallel octahedral planes. The shear evolved with increased strain so that the shear patterns looked like tetrahedral pyramids near each punch (Figure 3c), which confined the volumes, where end-face friction resulted in non-uniform hydrostatic compression and constrained deformation. Then one couple of the conjugate shear planes began to contribute more significantly (Figure 3d) resulting in appearing shear traces on the two adjacent lateral faces of the sample (see Figure 1).

When dislocations appeared on the surface, they produced steps, which served as nucleation sites for shear propagation from the crystal surface. As can be seen in Figure 3d, a Shockley

dislocation with the opposite Burgers vector moved along the same slip plane (indicated as "A"). This means that there were conditions for the nucleation of dislocations with different signs. Local excessive density of dislocations with the same sign resulted in long-range stresses. Interaction of the dislocations with opposite signs moving along the same plane led to their annihilation. In this way the conditions were created not only for further shear caused by stress concentrators (indicated as "B" in Figure 3d), but also for shear initiation in the regions located far from the punches of the testing machine, i.e., in the volume V_0 (Figure 1a).

The subsequent strain increase resulted in a decrease in the sample height. Deformation occurred by activation of new slip planes parallel to the initially activated ones (indicated as "C" in Figure 3d). This shear deformation resulted in generation of extrinsic stacking faults and twins in addition to intrinsic stacking faults. Load increasing led to propagation of shears in the bulk of the crystal, which initiated at both the punches and lateral faces of the crystal (planes "A" and "B" in Figure 4a). Shears along newly activated octahedral planes from the lower punch led to nucleation of deformation in the middle part of the single crystal. This deformation was accompanied by shears along the family of parallel slip planes, which manifested themselves in the formation of twin configurations ("A" in Figure 4b) and intrinsic stacking faults ("B" in Figure 4b). Active sliding along these planes resulted in increase of the sample width. The growing number of interacting dislocations gave rise to increasing probability of formation of dislocation barriers, in particular, a 1/6<110> Lomer–Cottrell barrier (colored pink in Figure 4 and thereafter).

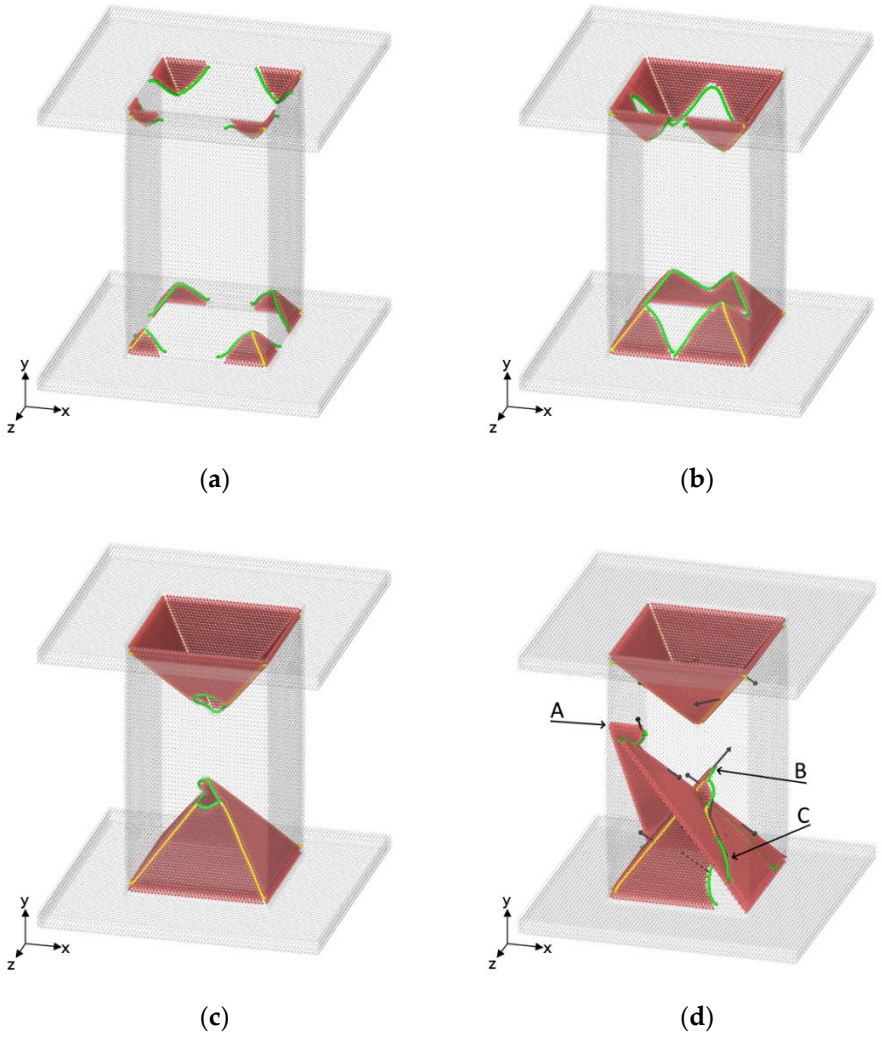

Figure 3. Deformation patterns in a <001> single crystal with h/d = 2 and {110} lateral faces at a sequentially increasing strain of (**a**) 7.39%; (**b**) 7.42%; (**c**) 7.44%; and (**d**) 7.51% (1/6<112> Shockley partial dislocations colored green, 1/3<001> Hirth dislocations colored yellow).

The development of deformation patterns indicates the emergence of new shear domains and a decrease in their dimensions. Shears continued to develop primarily near the punches and in the middle part of the sample. In addition, other shear systems acted in the local regions. This became especially pronounced when the height of the sample approached its width. Similar deformation behavior was observed during experimental compression of FCC metal single crystals with such orientation.

4.1.2. Sample with h/d = 1

The first stage of deformation of the nickel single crystals with h/d = 1 was similar to that of the higher sample. Initially, as in the above case, a 1/3<001> Hirth dislocation was generated along the intersection line of the adjacent planes, which started at the same vertex (Figure 5a). The sample geometry provided an intersection of slip planes, which started from the opposite punches, upon further decreasing h. At this stage, the result of shear along the slip plane was random and depended on the speed of the dislocation movement. Therefore, in the middle part of the sample the shear resulted from the action of slip systems associated with all eight stress concentrators. In this region the shear was constrained due to interaction of adjacent planes and formation of Hirth barriers ("A" in Figure 5c).

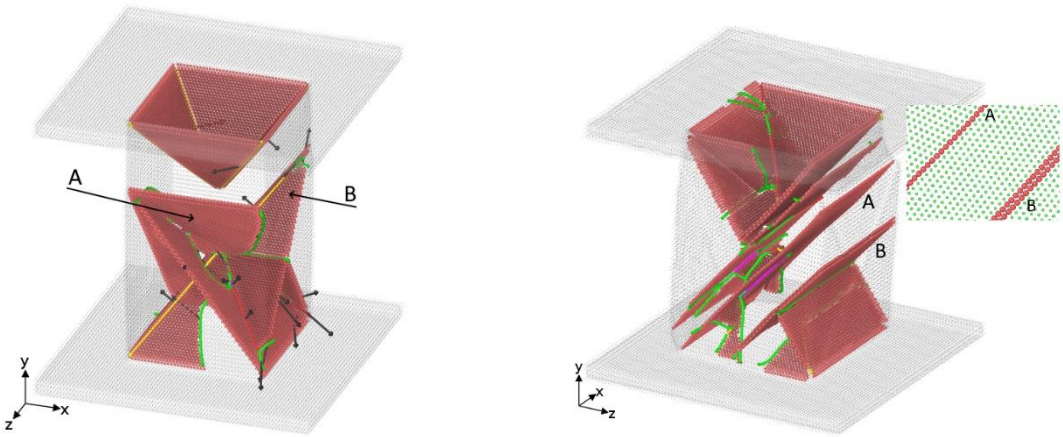

(**a**) (**b**)

Figure 4. Shear in a <001> single crystal with h/d = 2 and {110} lateral faces at a sequentially increasing strain of (**a**) 13.8%; (**b**) 16.9%. A and B in (**b**) indicate a twin boundary and an intrinsic stacking fault, respectively.

Along with consideration of shear development and interaction of dislocations belonging to different slip systems, which resulted in the formation of barriers or in shear only, it is necessary to draw attention to the difference in the patterns of principal stresses in the middle part of the sample and in the periphery regions, in the case of h/d=2. The hydrostatic compression pattern was realized in the middle part of the sample, which did not favor active plastic deformation. In addition, all shear planes in this region were constrained on both sides by the punches of the testing machine. In contrast, the non-uniform hydrostatic compression–tension pattern was realized in the periphery regions. This pattern was more favorable for active deformation, particularly as slip planes in this volume was constrained by the punch from only one side, and there were not constraints for shear towards the lateral faces.

Shear development in the periphery regions was characterized by the following specific features. In this case, shear along parallel slip planes did not result in the formation of Hirth barriers upon interaction of dislocations belonging to the slip systems of adjacent planes. Intrinsic and extrinsic stacking faults ("A" and "B" in Figure 5d, respectively) as well twins were formed in the periphery regions. Strong activation of different shear systems in different regions of the crystal

made possible formation of different types of dislocations. Along with the above-mentioned Shockley and Hirth dislocations, 1/3<111> Frank dislocations, 1/2<110> dislocations and 1/6<110> Lomer–Cottrell dislocations can be observed. Increasing strain primarily resulted in shear near the lateral faces.

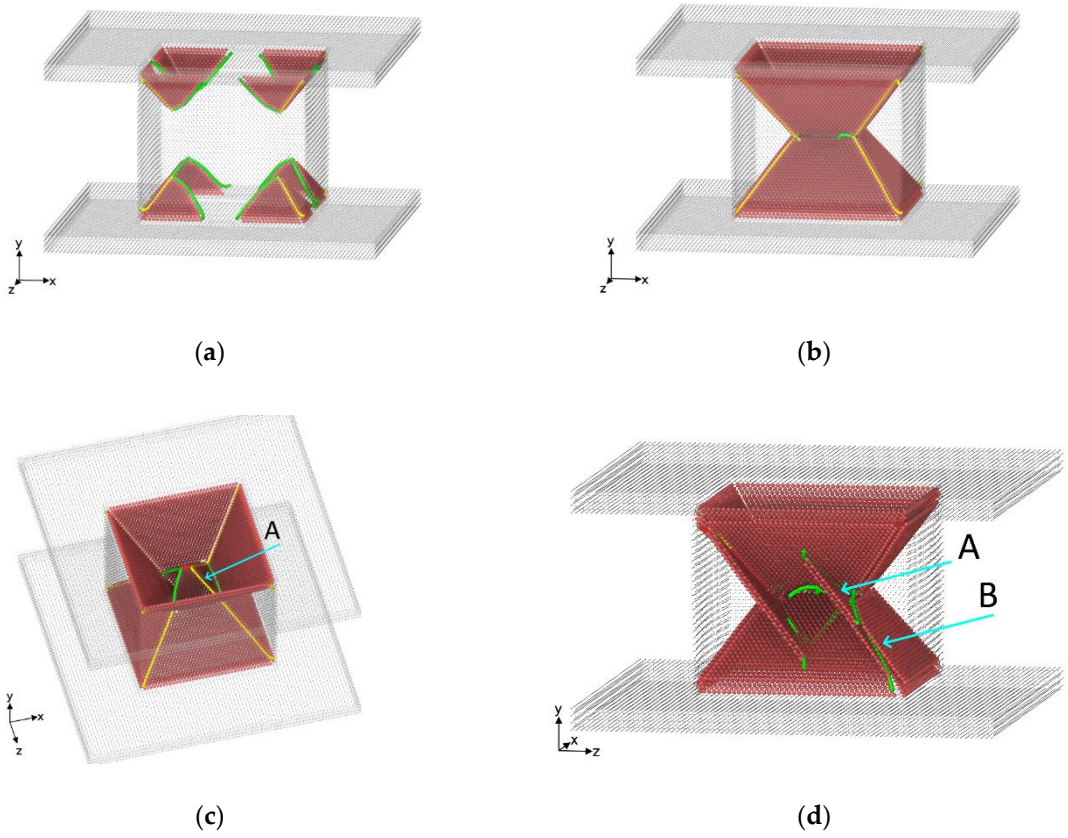

Figure 5. Deformation patterns in a <001> single crystal with h/d = 1 and {110} lateral faces at a sequentially increasing strain of (**a**) 7.0%; (**b, c**) 7.1%; (**d**) 8.7%.

4.1.3. Comparison with experiment

The above-described results of MD simulation of deformation behavior of FCC single crystals with different h/d ratios showed the evolution of shear systems and their interaction in different parts of the samples. A deformation relief pattern obtained for the simulated samples with different h/d ratios is depicted in Figure 6. It is in good agreement with the experimental results presented in Figures 7 and 8 [39]. In this work the deformation relief on the lateral faces of nickel single crystals at room temperature was studied systematically using optical and scanning microscopy. Nevertheless, they agree well with the data obtained for other metals with high and medium stacking fault energies. However, the homologous temperatures of deformation should be taken into account. These temperatures were close for Ni ($0.17T_m$) and Cu ($0.22T_m$) deformed at room temperature. Al single crystals were characterized by the higher homologous temperature of deformation $0.31T_m$. Therefore, in the case of Al, the shear pattern was similar, although small details were different (see Figures 9–11) [40].

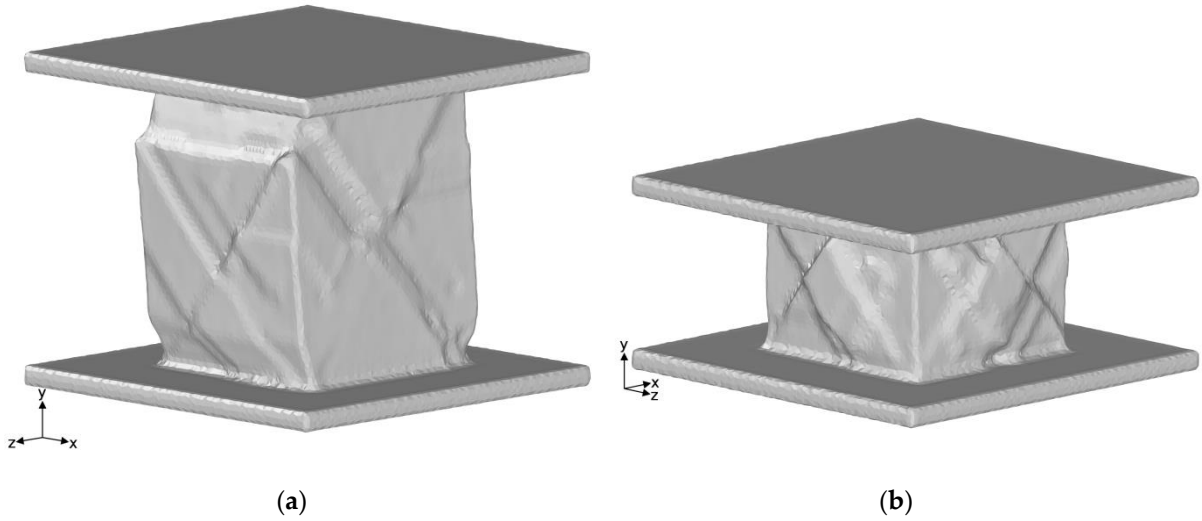

Figure 6. Surface deformation patterns in a simulated <001> Ni single crystal with {110} lateral faces: (**a**) h/d=2, ε=27%; (**b**) h/d=1, ε=22%.

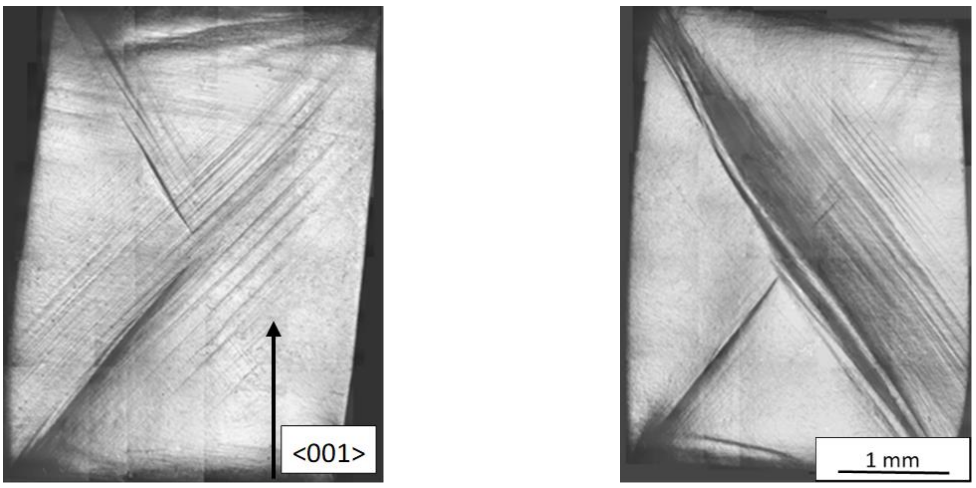

Figure 7. Surface deformation patterns on mutually perpendicular {110} lateral faces of a Ni single crystal. Compression was carried out along the <001> axis; h/d = 2, ε = 25%.

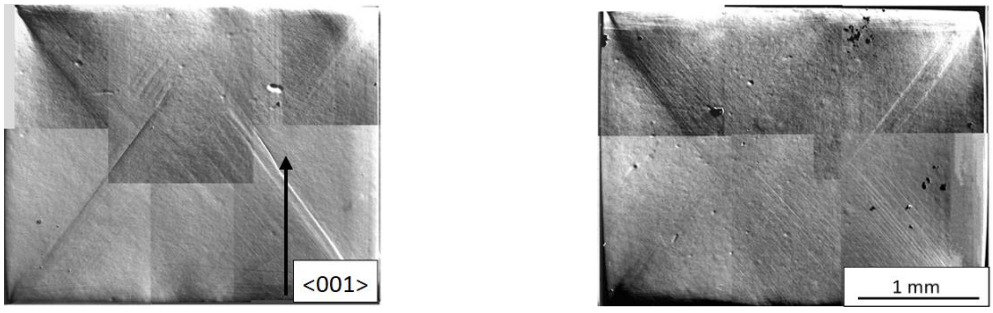

Figure 8. Surface deformation patterns on mutually perpendicular {110} lateral faces of a Ni single crystal. Compression was carried out along the <001> axis; h/d = 1, ε = 18%.

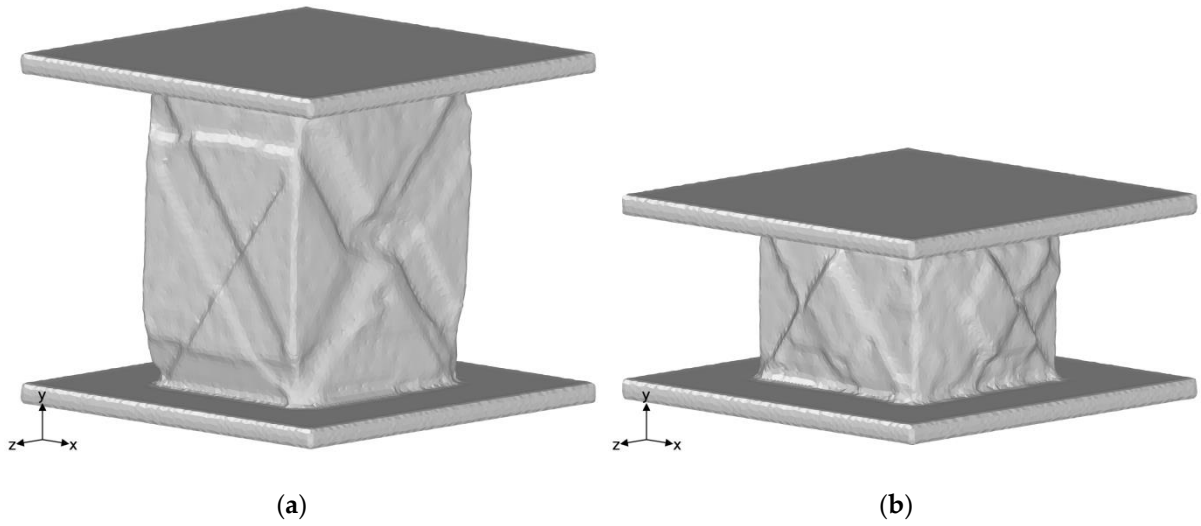

(**a**) (**b**)

Figure 9. Surface deformation patterns in a simulated <001> Al single crystal with {110} lateral faces: (**a**) h/d=2, ε=23.6%; (**b**) h/d=1, ε=19.2%.

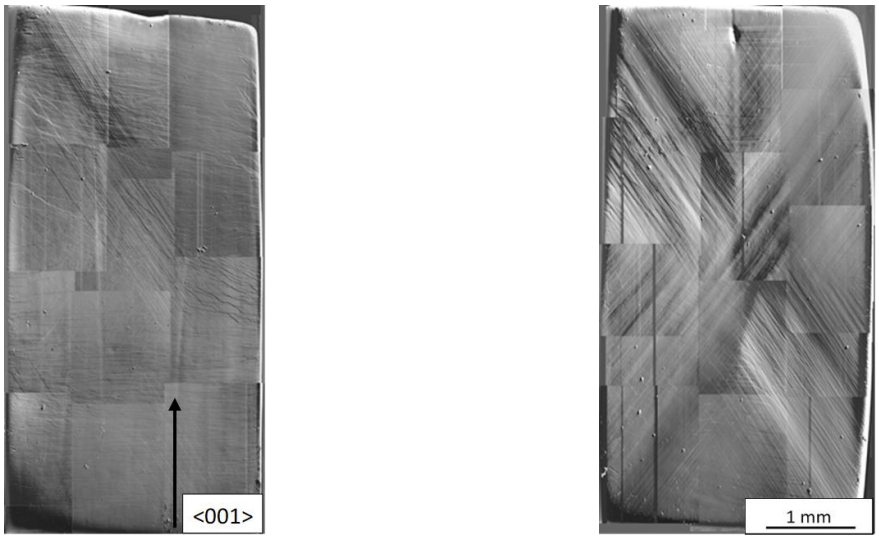

Figure 10. Deformation patterns on the {110} lateral faces of an Al single crystal. Compression was carried out along the <001> axis; h/d = 2, ε = 13%.

Figure 11. Deformation patterns on the {110} lateral faces of an Al single crystal. Compression was carried out along the <001> axis; h/d = 1, ε = 6%.

4.2. Single Crystals with the <001> Axis of Compression and {100} Lateral Faces

4.2.1. Sample with h/d = 2

In this case, shear initiated at all eight vertices of the sample. In each plane the shear was possible along two close-packed directions. As shown in Figure 12a, alternate shears in each system resulted in plane expansion. After a while, the shear planes activated at the same punch intersecting each other, resulting in the formation of a 1/3<001> Hirth dislocation (Figure 12b). Further shear was blocked in this region of the crystal and new shear initiated in the neighboring region. The shear plane passed through the middle of the crystal into its opposite part resulting in the formation of a twin-like defect in the middle part (Figure 12c,d). Tri- and tetrahedral configurations consisting of Lomer–Cottrell barriers were formed near this defect (see inset in Figure 12d), which disappeared after strain accumulation. Similar configurations have been experimentally observed [41] and simulated [42–45] earlier. Most of the Lomer–Cottrell barriers were observed in the middle part of the sample and near the punches. Along with the most active twin, which was located in the middle part, there was a twin along other system of slip planes. Deformation developed by means of the formation of new twins near the stress concentration sites (sample vertices). This resulted in a decrease in the sample height and an increasing in its width towards the lateral faces, which was the main mechanism of the subsequent deformation. Deformation and twin density became sufficient to identify defect clusters in the bulk of the material, which looked like dislocation cell structures at this stage of deformation.

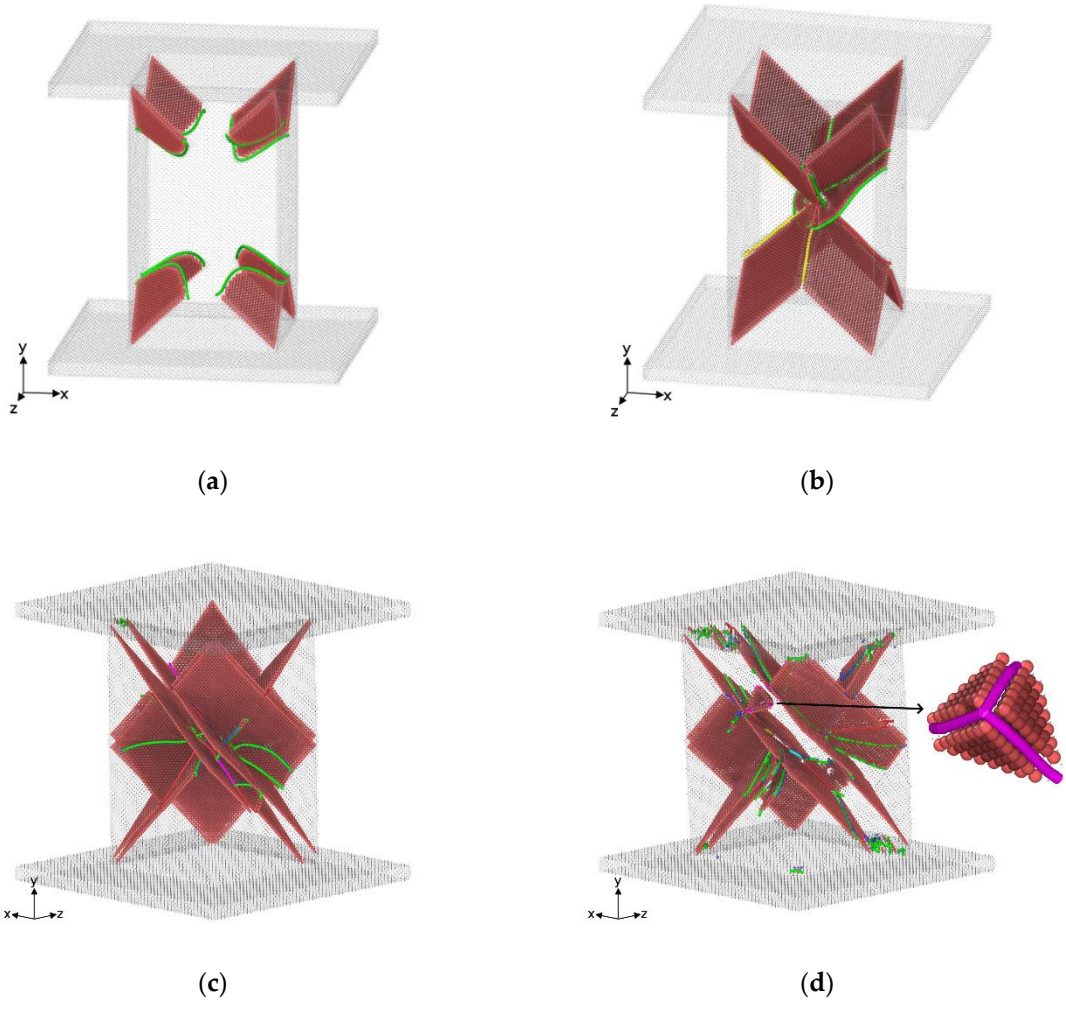

Figure 12. Surface deformation patterns in a simulated <001> single crystal with h/d=2 and {100} lateral faces at a sequentially increasing strain of (**a**) 7.92%; (**b**) 7.95%; (**c**) 9.32% and (**d**) 15.94%.

4.2.2. Sample with h/d = 1

In the sample with h/d = 1, shear also initiated at all eight vertices of the single crystal (Figure 13a) followed by intersection of shear planes starting at the opposite punches (Figure 13b). As mentioned above, in the case of the sample with h/d = 1 intersection of the shear planes starting at neighbor vertices near the lower punch was observed (Figure 3). This can be attributed to only the crystal geometric conditions (distance between stress concentrators).

The shear planes starting near the lower punch propagated close to the opposite punch. Stair-rod dislocations with the Burgers vector 1/3<001> were deposited along the intersection lines of the adjacent planes (Figure 13c). Twins and stacking faults were formed upon the subsequent deformation (Figure 13d). The decrease in the sample height was concerned with the deformation propagating towards the lateral surface. MD simulation exhibited that it was realized through two shear modes. The first mode was a shear along the planes parallel to the main shear planes with their increasing number (Figure 13e,f). The second one was a shear along two plane families, which was implemented in the regions, where the first shear mode was not activated (the outlined areas in Figure 13e). Both shear modes were realized in the periphery regions, where shears could come to the lateral faces, providing necessary shape changes.

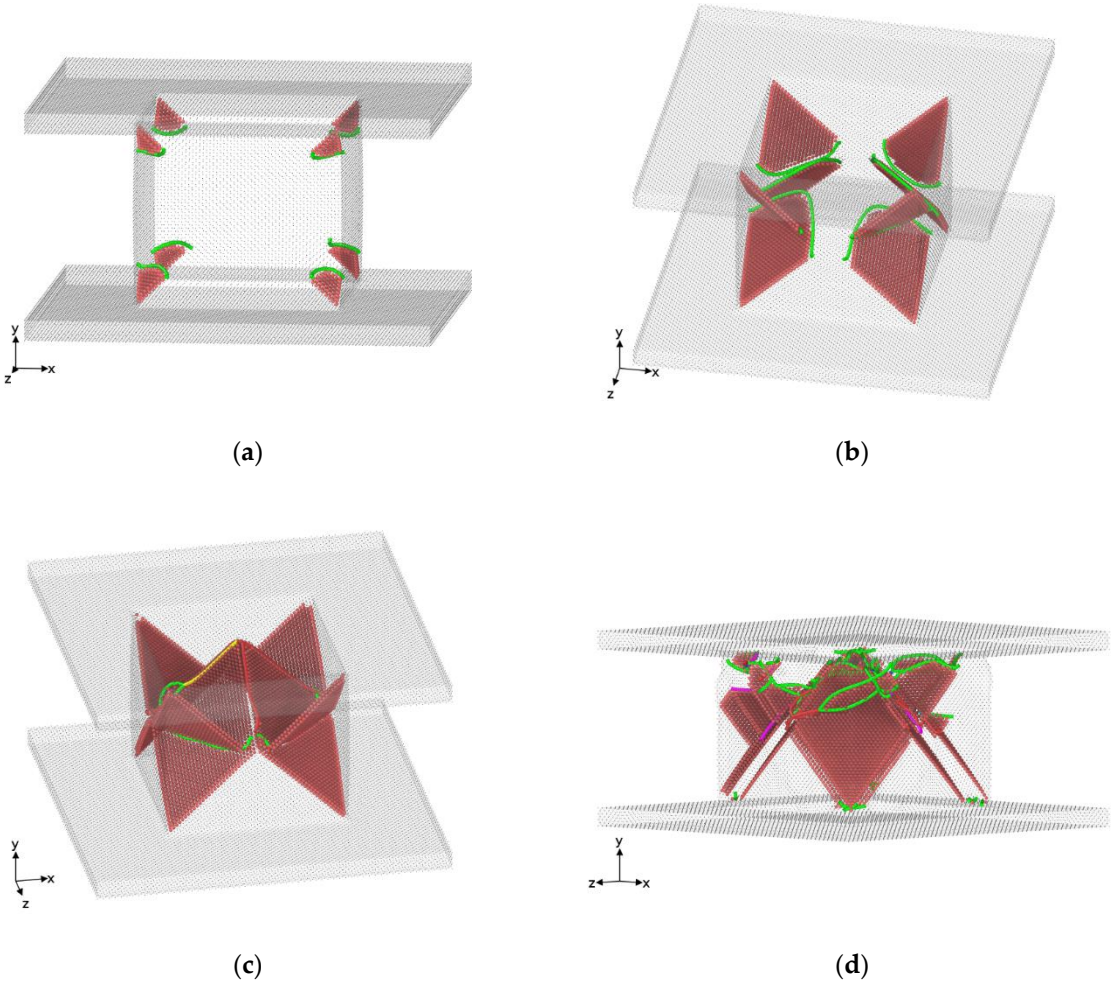

(**a**) (**b**)

(**c**) (**d**)

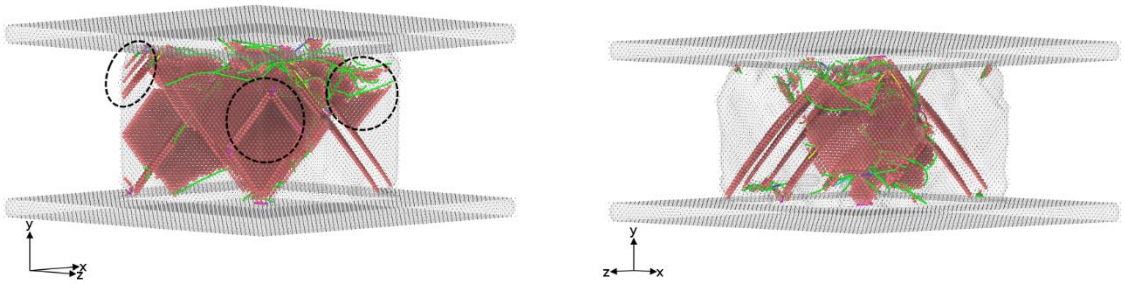

(**e**) (**f**)

Figure 13. Deformation patterns in a simulated <001> single crystal with h/d = 1 and {100} lateral faces at a sequentially increasing strain of (**a**) 7.79%; (**b**) 7.89%; (**c**) 7.94%; (**d**) 12.59%; (**e**) 14.2% and (**f**) 21.5%.

4.2.3. Comparison with Experiment

Deformation patterns in simulated <001> Ni single crystals with {110} lateral faces and different h/d ratios are shown in Figure 14. For the sample with h/d = 2 a family of octahedral shear planes propagating along the diagonal of the sample manifests itself on two perpendicular faces can be seen. This pattern well agrees with the crystallographic pattern of arrangement of octahedral planes in the sample (Figure 1) and with the experimental results (Figures 15 and 16). Similar results were also obtained for the same orientation of Al single crystals [46].

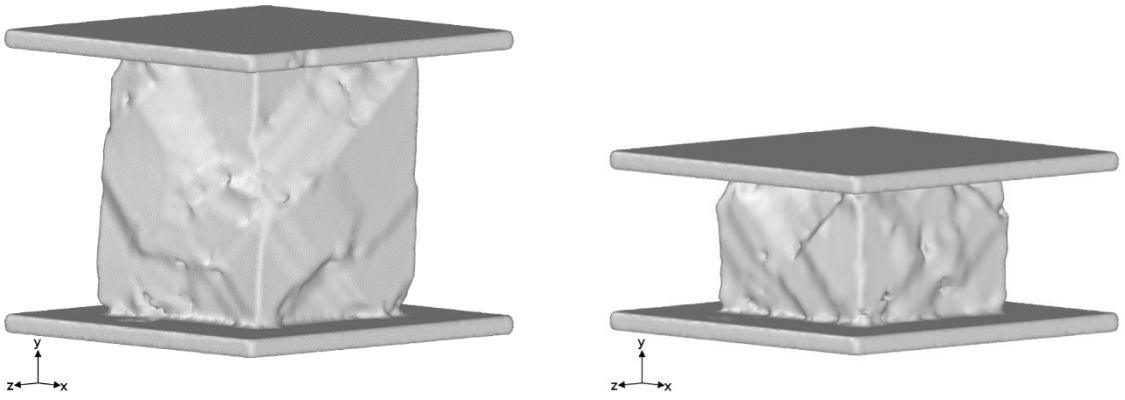

(**a**) (**b**)

Figure 14. Deformation patterns in a simulated <001> Ni single crystal with {100} lateral faces: (**a**) h/d=2, ε=27%; (**b**) h/d=1, ε=22%.

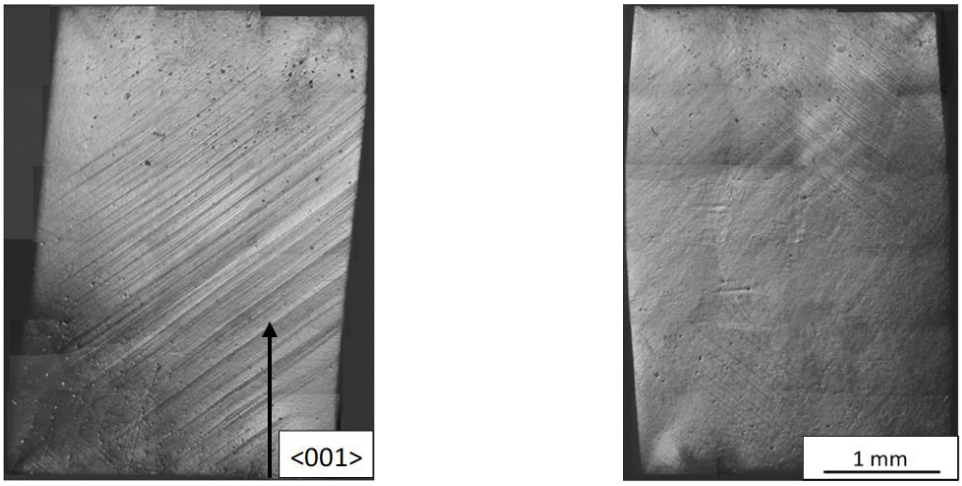

Figure 15. Deformation patterns on neighboring {100} lateral faces of a <001> Ni single crystal with h/d = 2. Compression was carried out along the <001> axis; ε = 22%.

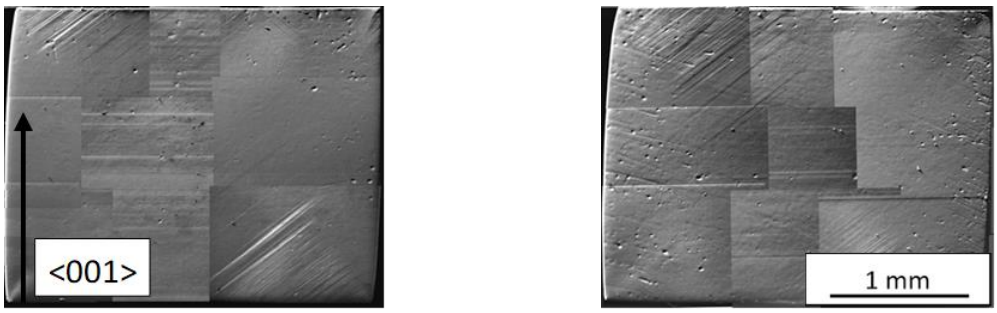

Figure 16. Deformation patterns on {100} lateral faces of a <001> Ni single crystal with h/d = 1; ε = 13%.

5. Discussion

The MD simulations showed that shear starts simultaneously at all vertices of the sample, which are the sites of stress concentration. The scheme of partitioning samples with different height-to-width ratios into domains depends largely on the geometry of positioning these basic stress concentrators. The simulation results were obtained for a case very close to the equiprobable shear starting at all eight concentrators. This ideal shear is difficult to realize in experiments because of failure to comply with the condition of the equiprobable shear along all four equiloaded planes, which can be caused by even small deviations in face parallelism or compression axis alignment. This is the main origin of the difference between the deformation patterns obtained in the experiments and MD simulations.

The results of the present and previous works exhibit that deformation patterns depend on local stress conditions and the possibility of shear deformation in the bulk of a single crystal. Shear deformation near the punches of the testing machine is constrained, while it can propagate towards the lateral faces. This is justified by the simulation results.

MD simulation makes it possible to estimate which dislocations are formed depending on the material (Ni or Al), crystallographic conditions (orientation of lateral faces) and sample geometry (various height-to-width ratios). The following findings can be drawn from the analysis of these factors performed using the data on fractions of different dislocations in Ni and Al samples listed in Table 1. The presented results indicate the following:

1. Shockley partial dislocations constitute the largest fraction. Their fraction in Ni is higher than in Al, except for the case of <001>{110} and h/d = 1. The number of sliding dislocations in Ni grows with the sample height. The inverse dependence is observed in Al.
2. The fraction of 1/3<001> Hirth barriers is higher in Ni as compared with Al. In contrast, the fraction of 1/6<110> stair-rod barriers is higher in Al as compared with Ni, except in the case of <001>{110} and h/d = 1. The number of barriers in Ni increases with decreasing sample height. The fraction of barriers in Al depends not only on the sample height but also on the orientation of the lateral faces.
3. Al is characterized by the presence of 1/3<111> Frank dislocations

Table 1. Fractions of different dislocations in Ni and Al samples subjected to 22% strain.

Dislocation type	<001>{110} h/d=2		<001>{110} h/d=1		<001>{100} h/d=2		<001>{100} h/d=1	
	Ni	Al	Ni	Al	Ni	Al	Ni	Al
1/2<110> Perfect	0.014	0.018	0.005	0.044	0.028	0.078	0.049	0.041
1/6<112> Shockley	0.787	0.602	0.756	0.893	0.750	0.708	0.734	0.713
1/6<110> Stair-rod	0.031	0.068	0.083	0.037	0.038	0.067	0.067	0.176
1/3<001> Hirth	0.026	0.017	0.071	0.011	0.015	0.009	0.057	0.003
1/3<111> Frank	0.012	0.167	0	0.014	0.030	0.046	0	0.028

The considered mechanisms of barrier formation are evidently concerned with the possibility of the interaction of dislocations belonging to different slip systems. The latter depends on crystallographic and geometrical factors governing shear activation, location and the number of basic stress concentrators, the possibility of cross-slip and homologous temperature of deformation. Some of these factors can be traced in the performed simulation, whereas the others are difficult to reveal, apparently due the simultaneous influence of several factors.

6. Conclusions

Using the principle of geometrical similarity, a comparison of shear patterns obtained by MD simulation with experimentally observed deformation relief was carried out for single crystals of pure FCC metals subjected to shear loading. Ni and Al samples in the form of tetragonal prisms with the highly symmetrical <001> axis of compression, {110} and {100} lateral faces and different height-to-width ratios were studied. In this case, the shear occurred by activation of eight equiloaded slip systems.

The simulation results showed that:

1. Shear initiates at basic stress concentrators (vertices of the sample). Decomposition of a crystal into deformation domains and interaction of dislocations belonging to different slip systems are determined by the positioning of shear planes relative to the basic stress concentrators and by their orientation relative to the lateral faces.
2. Shear activity depends on the value of the stress tensor and possibility of shear towards the lateral faces.
3. Gliding dislocations are most often observed. With a decreasing height of the Ni sample, the fraction of gliding dislocations is reduced, while the fraction of barriers grows. The opposite dependence is more often revealed in the Al single crystals. Crystallographic orientation of the lateral faces also has an influence on the barrier fraction. This effect is traced in aluminum.

Author Contributions: Conceptualization and writing, D.V.L. and A.I.D.; modeling, A.Y.N.; experiment, E.A.A. All authors have read and agreed to the published version of the manuscript.

Funding: This research was funded by the Program for Basic Scientific Research of the RAS on 2013–2020, Project III.23.2.4 and the Tomsk State University (TSU) competitiveness improvement program.

Conflicts of Interest: The authors declare no conflict of interest

References

1. Lychagin, D.V. Fragmentation of plastically deformed fcc metallic materials. *Phys. Mesomech.* **2006**, *9*, 95–105.
2. Lychagin, D.V.; Starenchenko, V.A.; Solov'eva, Y.V. Classification and scale hierarchy of structure elements in compression-strained fcc single crystals. *Phys. Mesomech.* **2006**, *9*, 63–72.
3. Dmitrieva, O.; Dondl, P.W.; Muller, S.; Raabe, D. Lamination microstructure in shear deformed copper single crystals. *Acta Mater.* **2009**, *57*, 3439–3449, doi:10.1016/j.actamat.2009.03.035.
4. Florando, J.N.; LeBlanc, M.M.; Lassila, D.H. Multiple slip in copper single crystals deformed in compression under uniaxial stress. *Scr. Mater.* **2007**, *57*, 537–540, doi:10.1016/j.scriptamat.2007.05.014.
5. Magid, K.R.; Florando, J.N.; Lassila, D.H.; LeBlanc, M.M.; Tamura, N.; Morris, J.W. Mapping mesoscale heterogeneity in the plastic deformation of a copper single crystal. *Philos. Mag.* **2009**, *89*, 77–107, doi:10.1080/14786430802558577.
6. Sangyul H.; KiTae K.; Heterogeneous deformation of Al single crystal: Experiments and finite element analysis. *Math. Mech. Solids.* **2011**, *16*, 652–661, doi:10.1177/1081286510387719.
7. LeBlanc, M.M.; Florando, J.N.; Lassila, D.H.; Schmidt, T.; Tyson, J. Image correlation applied to single crystal plasticity experiments and comparison to strain gage data. *Exp. Tech.* **2006**, *30*, 33–37, doi:10.1111/j.1747-1567.2006.00060.x.
8. Paul, H.; Maurice, C.; Driver, J.H. Microstructure and microtexture evolution during strain path changes of an initially stable Cu single crystal. *Acta Mater.* **2010**, *58*, 2799–2813, doi:10.1016/j.actamat.2009.12.055.
9. Han, J.-H.; Kim, D.-I.; Jee, K.-K.; Oh, K.H. Evolution of crystallographic orientations in an aluminum single crystal during tensile deformation. *Mater. Sci. Eng. A* **2004**, *387–389*, 60–63, doi:10.1016/j.msea.2004.01.083.
10. Lychagin, D.V.; Tarasov, S.Y.; Chumaevskii, A.V.; Alfyorova, E.A. Macrosegmentation and strain hardening stages in copper single crystals under compression. *Int. J. Plast.* **2015**, *69*, 36–53, doi:10.1016/j.ijplas.2015.01.007.
11. Alfyorova, E.A.; Lychagin, D.V. Self-organization of plastic deformation and deformation relief in FCC single crystals. *Mech. Mater.* **2018**, *117*, 202–213, doi:10.1016/j.mechmat.2017.11.011.
12. Zhang, L.; Lu, C.; Tieu, A.K. Nonlinear elastic response of single crystal Cu under uniaxial loading by molecular dynamics study. *Mater. Lett.* **2018**, *227*, 236–239, doi:10.1016/j.matlet.2018.05.094.
13. Tschopp, M.A.; McDowell, D.L. Influence of single crystal orientation on homogeneous dislocation nucleation under uniaxial loading. *J. Mech. Phys. Solids* **2008**, *56*, 1806–1830, doi:10.1016/j.jmps.2007.11.012.
14. Yildiz, Y.O.; Ahadi, A.; Kirca, M. Strain rate effects on tensile and compression behavior of nano-crystalline nanoporous gold: A molecular dynamic study. *Mech. Mater.* **2020**, *143*, 103338, doi:10.1016/j.mechmat.2020.103338.
15. Xiong, Q.; Kitamura, T.; Li, Z. Cylindrical voids induced deformation response of single crystal coppers during low-speed shock compressions: A molecular dynamics study. *Mech. Mater.* **2019**, *138*, 103167, doi:10.1016/j.mechmat.2019.103167.
16. Xiong, Q.; Kitamura, T.; Li, Z. Nanocrystallization in single-crystal copper under laser shock compression: A molecular dynamics study. *Mater. Sci. Eng. A* **2019**, *752*, 115–127, doi:10.1016/j.msea.2019.02.086.
17. Rawat, S.; Mitra, N. Molecular dynamics investigation of c-axis deformation of single crystal Ti under uniaxial stress conditions: Evolution of compression twinning and dislocations. *Comput. Mater. Sci.* **2018**, *141*, 19–29, doi:10.1016/j.commatsci.2017.09.015.
18. Xie, H.; Yu, T.; Yin, F. Tension–compression asymmetry in homogeneous dislocation nucleation stress of single crystals Cu, Au, Ni and Ni3Al. *Mater. Sci. Eng. A* **2014**, *604*, 142–147, doi:10.1016/j.msea.2014.03.018.
19. Weinberger, C.R.; Cai, W. Plasticity of metal wires in torsion: Molecular dynamics and dislocation dynamics simulations. *J. Mech. Phys. Solids* **2010**, *58*, 1011–1025, doi:10.1016/j.jmps.2010.04.010.
20. Sarvesha, R.; Gokhale, A.; Kumar, K.; Sharma, N.K.; Jain, J.; Singh, S.S. Effect of crystal orientation on indentation-induced deformation behavior of zinc. *Mater. Sci. Eng. A* **2020**, *776*, 139064, doi:10.1016/j.msea.2020.139064.
21. Dmitriev, A.I.; Kuznetsov, V.P.; Nikonov, A.Y.; Smolin, I.Y. Modeling of nanostructuring burnishing on different scales. *Phys. Mesomech.* **2014**, *17*, 243–249, doi:10.1134/S1029959914040018.
22. Li, J.; Fang, Q.; Liu, Y.; Zhang, L. Scratching of copper with rough surfaces conducted by diamond tip simulated using molecular dynamics. *Int. J. Adv. Manuf. Technol.* **2015**, *77*, 1057–1070, doi:10.1007/s00170-014-6536-6.

23. Su, H.; Tang, Q. Chip formation dependence of machining velocities in nano-scale by molecular dynamics simulations. *Sci. China Technol. Sci.* **2014**, *57*, 2426–2433, doi:10.1007/s11431-014-5708-9.
24. Shugurov, A.; Panin, A.; Dmitriev, A.; Nikonov, A. The effect of crystallographic grain orientation of polycrystalline Ti on ploughing under scratch testing. *Wear* **2018**, *408*, 214–221, doi:10.1016/j.wear.2018.05.013.
25. Dmitriev, A.I.; Nikonov, A.Y.; Shugurov, A.R.; Panin, A. V. Numerical study of atomic scale deformation mechanisms of Ti grains with different crystallographic orientation subjected to scratch testing. *Appl. Surf. Sci.* **2019**, *471*, 318–327, doi:10.1016/j.apsusc.2018.12.021.
26. Fung, K.Y.; Tang, C.Y.; Cheung, C.F. Molecular dynamics analysis of the effect of surface flaws of diamond tools on tool wear in nanometric cutting. *Comput. Mater. Sci.* **2017**, *133*, 60–70, doi:10.1016/j.commatsci.2017.03.006.
27. Zhang, P.; Zhao, H.; Shi, C.; Zhang, L.; Huang, H.; Ren, L. Influence of double-tip scratch and single-tip scratch on nano-scratching process via molecular dynamics simulation. *Appl. Surf. Sci.* **2013**, *280*, 751–756, doi:10.1016/j.apsusc.2013.05.056.
28. Sharma, A.; Datta, D.; Balasubramaniam, R. Molecular dynamics simulation to investigate the orientation effects on nanoscale cutting of single crystal copper. *Comput. Mater. Sci.* **2018**, *153*, 241–250, doi:10.1016/j.commatsci.2018.07.002.
29. Vegge, T.; Sethna, J.P.; Cheong, S.-A.; Jacobsen, K.W.; Myers, C.R.; Ralph, D.C. Calculation of quantum tunneling for a spatially extended defect: The dislocation kink in copper has a low effective mass. *Phys. Rev. Lett.* **2001**, *86*, 1546–1549, doi:10.1103/PhysRevLett.86.1546.
30. Gong, Y.; Zhu, Z.; Zhou, Y.; Sun, Y. Research on the nanometric machining of a single crystal nickel via molecular dynamics simulation. *Sci. China Technol. Sci.* **2016**, *59*, 1837–1846, doi:10.1007/s11431-016-0251-y.
31. Pekin, T.C.; Ding, J.; Gammer, C.; Ozdol, B.; Ophus, C.; Asta, M.; Ritchie, R.O.; Minor, A.M. Direct measurement of nanostructural change during in situ deformation of a bulk metallic glass. *Nat. Commun.* **2019**, *10*, 2445, doi:10.1038/s41467-019-10416-5.
32. Chen, K.; Shi, S.; Zhu, W.; Peng, X. Plastic deformation due to interfacial sliding in amorphous/crystalline nanolaminates. *Comput. Mater. Sci.* **2015**, *109*, 266–276, doi:10.1016/j.commatsci.2015.07.032.
33. Sainath, G.; Goyal, S.; Nagesha, A. Plasticity through de-twinning in twinned BCC nanowires. *Crystals* **2020**, *10*, 366, doi:10.3390/cryst10050366.
34. Alferova, E.; Lychagin, D.; Chernyakov, A. Research of stress field distribution in FCC-single crystal samples in compression. *Appl. Mech. Mater.* **2014**, *682*, 485–490, doi:10.4028/www.scientific.net/AMM.682.485.
35. Plimpton, S. Fast parallel algorithms for short-range molecular dynamics. *J. Comput. Phys.* **1995**, *117*, 1–19, doi:10.1006/jcph.1995.1039.
36. Mishin, Y.; Farkas, D.; Mehl, M.J.; Papaconstantopoulos, D.A. Interatomic potentials for monoatomic metals from experimental data and ab initio calculations. *Phys. Rev. B* **1999**, *59*, 3393–3407, doi:10.1103/PhysRevB.59.3393.
37. Stukowski, A. Visualization and analysis of atomistic simulation data with OVITO–the open visualization tool. *Model. Simul. Mater. Sci. Eng.* **2010**, *18*, 015012, doi:10.1088/0965-0393/18/1/015012.
38. Stukowski, A.; Bulatov, V. V; Arsenlis, A. Automated identification and indexing of dislocations in crystal interfaces. *Model. Simul. Mater. Sci. Eng.* **2012**, *20*, 085007, doi:10.1088/0965-0393/20/8/085007.
39. Lychagin, D.V.; Starenchenko, V.A.; Shaekhov, R.V.; Koneva, N.A.; Kozlov, E.V. Evolution of deformation in nickel single crystals with the [001] compression axis orientation and {110} lateral faces. *Phys. Mesomech.* **2005**, *8*, 79–87.
40. Lychagin, D. V.; Teplyakova, L.A. The primary macrofragmentation of shear in compressed aluminum single crystals. *Tech. Phys. Lett.* **2003**, *29*, 516–518, doi:10.1134/1.1589576.
41. Matsukawa, Y.; Zinkle, S.J. Dynamic observation of the collapse process of a stacking fault tetrahedron by moving dislocations. *J. Nucl. Mater.* **2004**, *329*, 919–923, doi:10.1016/j.jnucmat.2004.04.069.
42. Poletaev, G.M.; Starostenkov, M.D. Structural transformations of stacking fault tetrahedra upon the absorption of point defects. *Tech. Phys. Lett.* **2009**, *35*, 1–4, doi:10.1134/S1063785009010015.
43. Wang, H.; Xu, D.S.; Yang, R.; Veyssière, P. The formation of stacking fault tetrahedra in Al and Cu: I. Dipole annihilation and the nucleation stage. *Acta Mater.* **2011**, *59*, 1–9, doi:10.1016/j.actamat.2010.07.046.

44. Wang, H.; Xu, D.S.; Yang, R.; Veyssière, P. The formation of stacking fault tetrahedra in Al and Cu: II. SFT growth by successive absorption of vacancies generated by dipole annihilation. *Acta Mater.* **2011**, *59*, 10–18, doi:10.1016/j.actamat.2010.07.044.
45. Wang, H.; Xu, D.S.; Yang, R.; Veyssière, P. The formation of stacking fault tetrahedra in Al and Cu: III. Growth by expanding ledges. *Acta Mater.* **2011**, *59*, 19–29, doi:10.1016/j.actamat.2010.07.045.
46. Teplyakova, L.A.; Bespalova, I.V.; Lychagin, D.V. Laws of shear deformation in aluminum [001] single crystals with {100} lateral faces in compression. *Phys. Mesomech.* **2006**, *9*, 77–84. (In Russian)